

# Identification of the Magnetostatic Modes of Ferrimagnetic Resonant Spheres

P. FLETCHER, I. H. SOLT, JR., AND R. BELL  
*Hughes Aircraft Company, Culver City, California*

(Received December 15, 1958)

A detailed comparison between the magnetostatic theory and experimental observation is given. Both the resonant field and the intensity of the magnetostatic modes are compared. The disagreement between observation of resonant fields and the static theory is about 50 gauss for an yttrium iron garnet sphere 1.3 mm in diameter. Inclusion of the first-order propagation corrections reduces this disagreement to less than two gauss for 29 of the 31 modes that were compared. This increased accuracy allows both a more positive identification and a more accurate determination of  $g$ -factors. A comparison of the static theory of intensities with observation has likewise been made. The observed intensities are close to the predicted intensities for some lines and from 4 to 100 times greater for others.

## INTRODUCTION

SINCE the early experiments of White, Solt, and Mercereau,<sup>1</sup> and those of Dillon,<sup>2</sup> demonstrating the existence of magnetostatic modes in ferrimagnetic resonance, the theory of the magnetostatic modes of spheroids has been worked out with some considerable generality by Walker.<sup>3</sup> The purpose of the present paper is to compare in detail the experimentally observed resonant absorption pattern for spherical samples with the predictions of the magnetostatic theory and to point out the corrections to the simple theory which must be made in order to give an accurate description of the experimental facts. It will be shown that in addition to the perturbations of the pattern caused by nonideal experimental conditions, e.g., samples not quite spherical,<sup>4</sup> there exist mode shifts and "couplings" due to finite sample size which can cause serious ambiguities in mode identifications and errors in  $g$ -factor calculations unless recognized and taken into account. The Walker theory is also herein extended to include absorption and the use of absolute absorption intensity as a criterion for mode identification discussed.

## MAGNETOSTATIC MODE IDENTIFICATION

Recorder tracings of ferrimagnetic resonance of spheres that have been taken in the laboratory show over 65 discrete absorptions. The identification of this large number of modes proceeds by utilizing two calculable features of the absorptions: (1) their magnetic field for resonance, and (2) their relative and absolute intensities in rf configurations of various known geometries.<sup>5</sup> The use of these two criteria will be discussed in turn below.

<sup>1</sup> White, Solt, and Mercereau, *Bull. Am. Phys. Soc. Ser. II*, **1**, 12 (1956); R. L. White and I. H. Solt, *Phys. Rev.* **104**, 56-62 (1956).

<sup>2</sup> J. F. Dillon, Jr., *Bull. Am. Phys. Soc. Ser. II*, **1**, 125 (1956).

<sup>3</sup> L. R. Walker, *Phys. Rev.* **105**, 390-399 (1957).

<sup>4</sup> J. F. Dillon, Jr., *Phys. Rev.* **112**, 59 (1958).

<sup>5</sup> A. D. Berk and B. A. Lengyel, *Proc. Inst. Radio Engrs.* **43**, 11, 1587-91 (1955).

## MAGNETIC FIELDS FOR RESONANCE

### Theory

The theory of the magnetostatic modes of resonance of the general spheroid has been developed by Walker.<sup>3</sup> His results are mostly in general form, but Fletcher and Bell<sup>6</sup> have treated more extensively the case of spheres and have tabulated the explicit expressions for magnetic potentials, magnetic fields, and magnetization distribution for a large number of magnetostatic modes. The reader is referred to these articles for details on the definitions of the parameters and symbols used here. The various modes can be designated by the associated Legendre polynomial  $P_n^m(\xi_0)$  describing the magnetic potential and by an additional index  $r$  distinguishing between the modes corresponding to the various roots of the resonance-condition equation

$$\xi_0 \left[ \frac{P_n^r(\xi_0)}{P_n^m(\xi_0)} \right] + n + 1 \pm m\nu = 0. \quad (1)$$

A plot of the fields for resonance for the modes with  $n$  up to 5 is given in Fig. 1. The plot also contains a line indicating the manner in which the modes are traversed as  $H_0$  is varied. The traversal line is drawn to correspond to an experiment conducted on a sphere with  $\omega/(\gamma 4\pi M) = 1.94$ .

### Experimental Results

In Fig. 2 are reproduced tracings of the absorption due to an yttrium iron garnet (YIG) single-crystal sphere 1.3 mm in diameter at 9709.7 Mc/sec and at 30.1°C. Tracings at two gains differing by a factor of about 100 are given so that both large and small absorptions can be displayed. The mode identifications and resonant fields are also indicated. Over 65 resonances are distinguishable and nearly 40 have been identified. The observed resonant fields for the modes with  $n$  up to 5 are given in Table I, together with the resonant fields predicted by the simple theory described above. There are discrepancies as large as 43 gauss between

<sup>6</sup> P. C. Fletcher and R. O. Bell, *J. Appl. Phys.* **30**, 687 (1959).

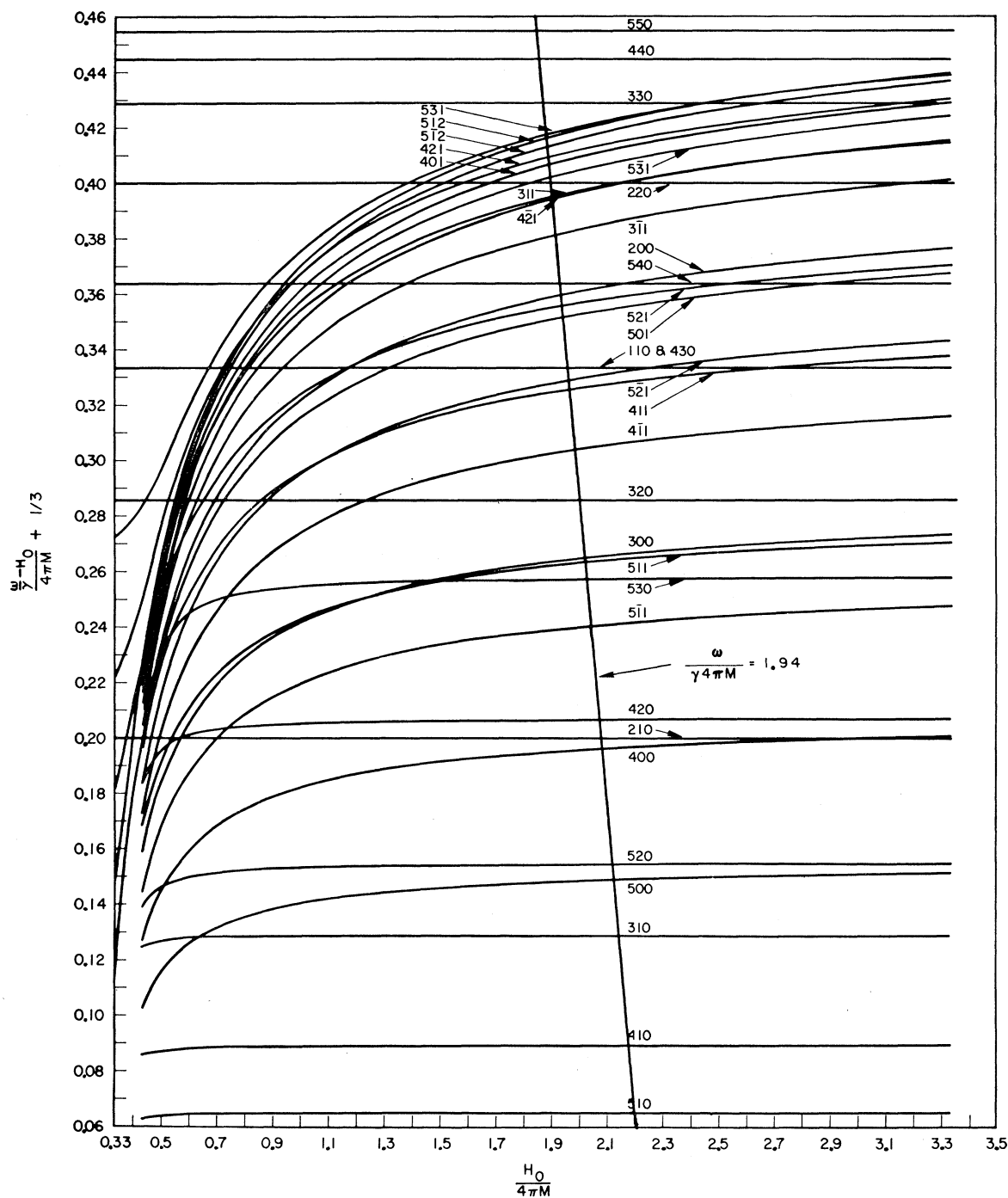


FIG. 1. Plot of  $(\omega/\gamma - H_i)/4\pi M$  versus  $H_0/4\pi M$  for modes with  $n$  up to 5.

observed and calculated fields. For samples with larger  $4\pi M$ , for example, MnZn ferrite, discrepancies as large as 150 gauss have been noted. The value of  $\omega/\gamma$  has been chosen so that the discrepancies decrease with increasing  $n$  for reasons which will become evident below.

### Propagation Effects

There are two corrections to the simple theory which are introduced by the breakdown of the magnetostatic condition. The first is a shift of all resonant absorptions toward the high-field direction. This shift has been

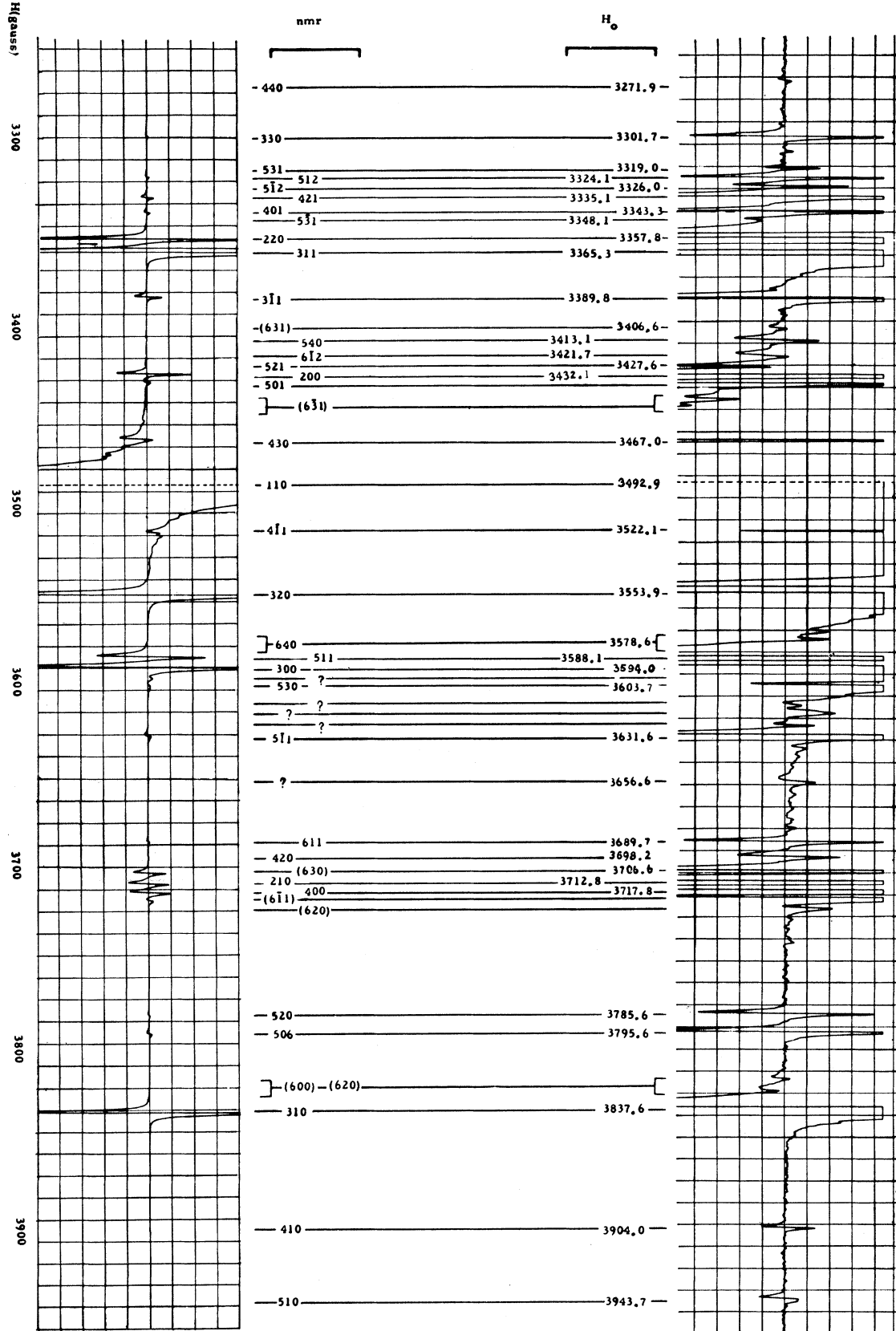


FIG. 2. Tracings of  $\Delta(1/Q)$  versus magnetic field; (a) maximum signal/noise; (b) gain/100 for YIG single crystal in arbitrary orientation.

TABLE I. Comparison of observed resonant fields with calculated resonant fields with and without corrections for single crystal YIG at 30.1°C and at 9709.7 Mc/sec. Assumed constants:  $\omega/\gamma = 3445.0$  gauss,  $4\pi M = 1773.5$  gauss,  $\Delta H_{\text{anisotropy}} = 17.8$  gauss.

| Mode | $H_{\text{simple theory}}$<br>(gauss) | $H_{\text{corr}}$<br>(gauss) | $H_{\text{obs}}$<br>(gauss) | $\Delta$ (gauss) |
|------|---------------------------------------|------------------------------|-----------------------------|------------------|
| 440  | 3259.1                                | 3270.0                       | 3271.9                      | -1.9             |
| 330  | 3287.3                                | 3301.4                       | 3301.7                      | -0.3             |
| 531  | 3308.2                                | 3318.3                       | 3319.0                      | -0.7             |
| 512  | 3310.5                                | 3324.2                       | 3324.1                      | +0.1             |
| 512  | 3315.6                                | 3329.8                       | 3329.5                      | +0.3             |
| 421  | 3322.3                                | 3333.9                       | 3335.1                      | -1.2             |
| 401  | 3327.8                                | 3343.2                       | 3343.3                      | -0.1             |
| 531  | 3335.3                                | 3348.4                       | 3348.1                      | +0.3             |
| 220  | 3338.0                                | 3358.5                       | 3357.8                      | +0.7             |
| 311  | 3347.7                                | 3365.5                       | 3365.3                      | +0.2             |
| 311  | 3371.7                                | 3390.3                       | 3389.8                      | +0.5             |
| 540* | 3406.5                                | 3417.0                       | 3413.1                      | +3.9             |
| 521* | 3416.7                                | 3426.5                       | 3427.6                      | -1.1             |
| 200  | 3410.2                                | 3432.4                       | 3432.1                      | +0.3             |
| 501  | 3424.3                                | 3435.9                       | 3436.8                      | -0.9             |
| 430  | 3456.2                                | 3467.5                       | 3467.6                      | +0.1             |
| 110  | 3456.2                                | 3492.8                       | 3493.3                      | -0.5             |
| 411  | 3508.7                                | 3521.7                       | 3522.1                      | -0.4             |
| 320  | 3540.6                                | 3553.7                       | 3553.9                      | -0.2             |
| 511  | 3580.7                                | 3587.7                       | 3588.3                      | -0.6             |
| 300  | 3577.7                                | 3593.5                       | 3594.0                      | -0.5             |
| 530  | 3591.2                                | 3602.1                       | 3603.7                      | -1.4             |
| 511  | 3620.8                                | 3631.4                       | 3631.6                      | -0.2             |
| 420  | 3681.0                                | 3698.1                       | 3698.2                      | -0.1             |
| 210  | 3692.6                                | 3713.1                       | 3712.8                      | +0.3             |
| 400  | 3699.2                                | 3717.2                       | 3717.8                      | -0.6             |
| 520  | 3773.2                                | 3785.0                       | 3785.6                      | -0.6             |
| 500  | 3782.8                                | 3795.1                       | 3795.6                      | -0.5             |
| 310  | 3818.5                                | 3837.2                       | 3837.6                      | -0.4             |
| 410  | 3889.1                                | 3903.8                       | 3904.0                      | -0.2             |
| 510  | 3931.9                                | 3939.0                       | 3943.7                      | -3.8             |
| 421  | falls on 311                          |                              |                             |                  |
| 411  | falls on 430                          |                              |                             |                  |
| 521  | falls on 110                          |                              |                             |                  |
| 550  | too weak to be seen                   |                              |                             |                  |

\* Lines are weakly coupled.

observed in the uniform mode by Artman<sup>7</sup> and calculated theoretically by Hurd<sup>8</sup> and Mercereau.<sup>9</sup> The shift for the other modes has not been calculated but can be found experimentally by the following means. Since the shift, to first order, is proportional to  $M$ , one can change the temperature to change  $M$ , plot  $\omega/\gamma$  versus  $M$ , and find the intercept for  $M=0$  giving  $(\omega/\gamma)_0$ . This procedure has been carried out for the sample sphere of YIG 1.3 mm in diameter. The results are shown in Fig. 3. The slopes of these lines can be used to estimate the propagation shift in other samples and are listed in Table II for modes up to  $n=5$ . Because of the difference of the dielectric constant between YIG and MnZn ferrite, the slopes of the propagation shift for MnZn are somewhat different. The value of  $(\omega/\gamma)_0$  obtained in this fashion is the one appropriate to the magnetostatic picture and should be used in obtaining a magnetic  $g$ -factor. Since the shift seems to decrease with increasing  $n$ , the first mode index, the higher lines agree better. The fourth column in Table I shows the cal-

culated resonant fields, including propagation corrections obtained in this fashion; it can be seen that quite satisfactory agreement between observed and calculated fields results.

The second effect that propagation has on the resonant field may occur when the resonant fields of two modes approach degeneracy. When this occurs, each mode apparently repels the other in a manner similar to the behavior of two coupled tuned circuits near degeneracy and this effect is therefore called mode coupling. When propagation is taken into account, the modes are no longer orthogonal, that is, the normal coordinates become scrambled and an rf field formerly driving one mode uniquely will now drive both. This effect has been reported by Solt and White<sup>10</sup> and described more completely by Fletcher and Solt.<sup>11</sup> Although with yttrium iron garnets the magnetization is so small that no dramatic examples of coupling are shown in Table I, one small example is evident. The 540 mode is pushed away from the 521 mode. As has been pointed out,<sup>11</sup> the selection rule for this coupling is, experimentally,  $\Delta m=0, 2, \dots$ ;  $\Delta n=0, 2, 4, \dots 2p$ ;  $\Delta r=0, 1, 2, \dots$ .

## ABSORPTION INTENSITY

### Theory

In the original derivation of the magnetostatic mode theory by Walker, no loss terms were included in the gyromagnetic equations, and hence no absorption intensities could be calculated. Inasmuch as the absorption intensity of the various modes as a function of rf configuration has provided a useful means of mode identification,<sup>1</sup> it was deemed desirable to extend the theory to include damping terms and to calculate absolute absorption intensities.

Only the uniform precessional mode has been treated

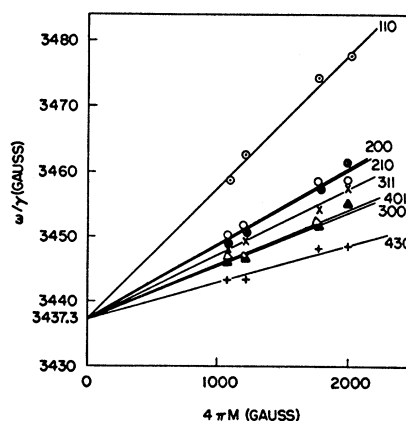


FIG. 3.  $\omega/\gamma$  versus  $4\pi M$  for a few of the magnetostatic modes. The data are for a 1.3-mm diameter YIG at 9688 Mc/sec.

<sup>7</sup> J. Artman, Lincoln Laboratories Group Report M35-54 (unpublished).

<sup>8</sup> R. A. Hurd, Can. J. Phys. **36**, 1072 (1958).

<sup>9</sup> J. E. Mercereau, J. Appl. Phys. **30**, 184S (1959).

<sup>10</sup> I. H. Solt and R. L. White, Bull. Am. Phys. Soc. Ser. II, **2**, 22 (1957).

<sup>11</sup> P. C. Fletcher and I. H. Solt, J. Appl. Phys. **30**, 181S (1959).

in the literature in a manner that includes damping. Therefore a sketch of the method of calculation for the more general modes will be presented here.

It has been shown<sup>5</sup> in several places that the rf absorption due to a small magnetic sample in a microwave cavity may be expressed as

$$\Delta(1/Q) = -\text{Im}\left(\frac{1}{2\pi E} \int 4\pi \mathbf{m} \cdot \mathbf{h}_0^* dV\right), \quad (2)$$

where  $\Delta(1/Q)$  is the change in the reciprocal of the  $Q$  of the microwave cavity due to the ferrimagnetic absorption,  $\mathbf{m}$  is the rf magnetization in the ferrite,  $\mathbf{h}_0$  is the applied rf field without a ferrite,  $E$  is the total energy stored, and  $V$  is the volume of the ferrite. The total energy  $E$  is assumed to be constant in all these calculations, i.e., energy stored in the induced rf fields internal and external to the ferrite is assumed to be small compared with the stored energy of the cavity. This assumes that the sample is small compared with the cavity, an assumption implicit in Eq. (2).

To calculate  $\Delta(1/Q)$  for the higher-order magnetostatic modes, it is necessary to calculate explicitly the rf magnetizations  $\mathbf{m}$  and the nonuniform components of the rf field  $\mathbf{h}_0$  appropriate to each mode. The rf magnetization  $\mathbf{m}$ , as calculated implicitly by Walker<sup>3</sup> and explicitly by Fletcher and Bell,<sup>6</sup> was derived by using a loss-free gyromagnetic equation and hence must lead to zero change in  $Q$ . It is necessary therefore to re-derive the magnetizations by starting with a gyromagnetic equation including damping:

$$\partial \mathbf{M} / \partial t = \gamma (\mathbf{M} \times \mathbf{H}) + \text{damping term}, \quad (3)$$

where  $\gamma$  is the gyromagnetic ratio,  $\mathbf{H}$  is the total magnetic field and  $\mathbf{M}$  is the total magnetization. Two types of damping have been commonly postulated in the literature; they lead to substantially different ex-

TABLE II. Propagation slopes,  $\Delta(\omega/\gamma)/\Delta(4\pi M)$ , for YIG sphere 1.3 mm in diameter at 9688.0 Mc/sec.

| Mode | Slope <sup>a</sup>  | Mode | Slope <sup>a</sup>  |
|------|---------------------|------|---------------------|
| 110  | 2.06                | 400  | 1.01                |
| 220  | 1.15                | 401  | 0.86                |
| 210  | 1.15                | 550  | (0.55) <sup>b</sup> |
| 200  | 1.25                | 540  | 0.59                |
| 330  | 0.79                | 530  | 0.61                |
| 320  | 0.74                | 531  | 0.57                |
| 310  | 1.05                | 531  | 0.74                |
| 311  | 1.00                | 520  | 0.66                |
| 311  | 1.05                | 521  | 0.55                |
| 300  | 0.89                | 521  | (0.60) <sup>b</sup> |
| 440  | 0.61                | 510  | 0.45                |
| 430  | 0.63                | 511  | 0.39                |
| 420  | 0.96                | 511  | 0.59                |
| 421  | 0.68                | 512  | 0.77                |
| 421  | (0.85) <sup>b</sup> | 512  | 0.80                |
| 410  | 0.83                | 500  | 0.69                |
| 411  | (0.65) <sup>b</sup> | 501  | 0.65                |
| 411  | 0.73                |      |                     |

<sup>a</sup> All values are to be multiplied by  $10^{-2}$ .

<sup>b</sup> Parentheses indicate estimated values.

TABLE III. Assumed amplitudes of the rf field for various positions of the sphere in the cavity. Code:  $k_1 = l\pi/W$ ,  $k_3 = n\pi/L$ ,  $k^2 = k_1^2 + k_3^2$ ,  $W$  = width of cavity,  $L$  = length of cavity,  $l$  and  $n$  = cavity integers.

| Rf configuration | Dc mag. field <sup>a</sup> | Rf amplitudes   |
|------------------|----------------------------|---|
| Fig. 4A          | $\oplus$                   | $A_2^2 = (k_1 12k^2)(k_1^2 - k_3^2)$ , $A_2^0 = \frac{1}{3}k_1$                                     |
| Fig. 4B          | $\oplus$                   | $A_1^1 = k_1 k_3 / k^2$ , $A_3^3 = (k_1 k_3 / 360k^2)(k_3^2 - 3k_1^2)$ ,<br>$A_3^1 = k_1 k_3 / 180$ |
| Fig. 4C          | $\oplus$                   | $A_1^1 = k_1^2 / k^2$ , $A_3^1 = k_1^2 / 180$ ,<br>$A_3^3 = (k_1^2 / 360k^2)(3k_3^2 - k_1^2)$       |
| Fig. 4D          | $\oplus$                   | $A_2^2 = \frac{1}{6}k_1^2 k_3 / k^2$  |
| Fig. 4A          | $\uparrow$                 | $A_2^1 = (k_1 / 6k^2)(3k_1^2 - k_3^2)$  |
| Fig. 4B          | $\uparrow$                 | $A_3^0 = (k_1 k_3 / 30k^2)(4k_1^2 - k_3^2)$ ,<br>$A_3^2 = (k_1 k_3 / 180k^2)(k_3^2 - 2k_1^2)$       |
| Fig. 4C          | $\uparrow$                 | Large $A_1^1$   |
| Fig. 4D          | $\uparrow$                 | $A_2^0 = k_1^2 k_3 / 2k^2$ , $A_2^2 = k_1^2 k_3 / 12k^2$  |

<sup>a</sup>  $\oplus$  indicates that the dc magnetic field is perpendicular to the broad side of the X-band cavity;  $\uparrow$  that it is parallel.

pressions for line widths. These are the Bloch-Bloembergen<sup>12</sup> and Landau-Lifshitz<sup>13</sup> forms and may be written, respectively, as

$$\text{Landau-Lifshitz: } \frac{\alpha}{|\mathbf{M}|} \left( \mathbf{M} \times \frac{\partial \mathbf{M}}{\partial t} \right), \quad (4)$$

$$\text{Bloch-Bloembergen: } -\left( \frac{\mathbf{M} - \mathbf{M}_0}{\tau} \right) + \frac{|\mathbf{M}|}{|\mathbf{H}|} \frac{\mathbf{H}}{\tau}.$$

The parameters  $\kappa$  and  $\nu$  in the expressions for  $\mathbf{m}$ ,

$$4\pi m_x = \kappa h_x - i\nu h_y, \quad 4\pi m_y = i\nu h_x + \kappa h_y, \quad (5)$$

become

Landau-Lifshitz:

$$\kappa = \left( H_i - \frac{i\alpha\omega}{\gamma} \right) 4\pi M / \left[ \left( H_i - \frac{i\alpha\omega}{\gamma} \right)^2 + \left( \frac{\omega}{\gamma} \right)^2 \right] \quad (6)$$

$$\nu = \left( \frac{\omega}{\gamma} \right) 4\pi M / \left[ \left( H_i - \frac{i\alpha\omega}{\gamma} \right)^2 + \left( \frac{\omega}{\gamma} \right)^2 \right],$$

Bloch-Bloembergen:

$$\kappa = H_i 4\pi M / \left[ \left( i - \frac{1}{\gamma\tau} \right)^2 + H_i^2 \right]$$

$$\nu = \left( \frac{\omega}{\gamma} \right) 4\pi M / \left[ \left( i - \frac{1}{\gamma\tau} \right)^2 + H_i^2 \right]$$

and the rf  $\mathbf{m}$  for Eq. (2) is now totally defined.

Next, the components of the rf field  $\mathbf{h}_0$  at the ferrite in the cavity must be determined. All experiments reported here have been done in a rectangular cavity using a  $TE_{10n}$  cavity mode. As a first approximation one can expand the rf fields about the center of the sphere. Several cavity positions were used. Rough cor-

<sup>12</sup> See, for instance, N. Bloembergen, Proc. I. R. E. 44, 1259 (1956).

<sup>13</sup> See, for instance, H. Suhl, J. Phys. Chem. Solids 1, 209 (1956).

TABLE IV. Values of  $\Delta(1/Q)$  using the Landau-Lifshitz damping, assuming small damping.

| Mode | $\Delta(1/Q)$   |
|------|---|
| 110  | $\frac{1}{2} \frac{\omega\alpha}{\gamma} \frac{4\pi M}{E} (A_1)^2 V \left/ \left[ \left( H_0 - \frac{\omega}{\gamma} \right)^2 + \left( \frac{\omega\alpha}{\gamma} \right)^2 \right] \right.$  |
| 220  | $\frac{36}{5} \frac{\omega\alpha}{\gamma} \frac{4\pi M}{E} (A_2)^2 V a^2 \left/ \left[ \left( H_0 - \frac{\omega}{\gamma} + \frac{4\pi M}{15} \right)^2 + \left( \frac{\omega\alpha}{\gamma} \right)^2 \right] \right.$   |
| 210  | $\frac{9}{10} \frac{\omega\alpha}{\gamma} \frac{4\pi M}{E} (A_2)^2 V a^2 \left/ \left[ \left( H_0 - \frac{\omega}{\gamma} - \frac{8\pi M}{15} \right)^2 + \left( \frac{\omega\alpha}{\gamma} \right)^2 \right] \right.$   |
| 200  | $\frac{1}{5} \frac{\omega\alpha}{\gamma} \frac{4\pi M}{E} (A_2^0)^2 V a^2 \left( H_0 + \frac{4M}{15} \right) \left/ \left( H_0 + \frac{28M}{15} \right) \right.$<br>$\left[ \left( H_0 - \frac{4\pi M}{3} \right)^2 \left( H_0 + \frac{28\pi M}{15} \right)^2 - \frac{\omega^2}{\gamma^2} \right]$<br>$+ \left( \frac{\omega\alpha}{\gamma} \right)^2 \left( H_0 + \frac{4\pi M}{15} \right)^2 \left/ \left[ \left( H_0 - \frac{4\pi M}{3} \right) \left( H_0 + \frac{28\pi M}{15} \right) \right] \right.$           |
| 330  | $\frac{3240}{14} \frac{\omega\alpha}{\gamma} \frac{4\pi M}{E} (A_3)^2 V a^4 \left/ \left[ \left( H_0 - \frac{\omega}{\gamma} + \frac{8\pi M}{21} \right)^2 + \left( \frac{\omega\alpha}{\gamma} \right)^2 \right] \right.$  |
| 320  | $\frac{360}{14} \frac{\omega\alpha}{\gamma} \frac{4\pi M}{E} (A_3)^2 V a^4 \left/ \left[ \left( H_0 - \frac{\omega}{\gamma} + \frac{4\pi M}{21} \right)^2 + \left( \frac{\omega\alpha}{\gamma} \right)^2 \right] \right.$   |
| 300  | $\frac{18}{70} \frac{\omega\alpha}{\gamma} \frac{4\pi M}{E} (A_3^0)^2 V a^4 \left( H_0 - \frac{4\pi M}{21} \right) \left/ \left( H_0 + \frac{20\pi M}{21} \right) \right.$<br>$\left[ \left( H_0 - \frac{4\pi M}{3} \right)^2 \left( H_0 + \frac{20\pi M}{21} \right)^2 - \frac{\omega^2}{\gamma^2} \right]$<br>$+ \left( \frac{\omega\alpha}{\gamma} \right)^2 \left( H_0 - \frac{4\pi M}{21} \right)^2 \left/ \left[ \left( H_0 - \frac{4\pi M}{3} \right) \left( H_0 + \frac{20\pi M}{21} \right) \right] \right.$ |

relations can be made between these field components and the magnetic-field configurations matching onto the various magnetostatic modes and hence appropriate to the derived theory. Table III gives the  $\mathbf{h}_0$  amplitudes matching onto several of the magnetostatic modes for several cavity configurations.

Finally, the  $\mathbf{m}$  and  $\mathbf{h}_0$  expressions derived in the two preceding steps are introduced into Eq. (2) and explicit expressions for  $\Delta(1/Q)$  obtained. These expressions are listed in Tables IV for the Landau-Lifshitz damping mechanism for the 110, 220, 210, 200, 330, 320, and 300 modes. The results using Bloch-Bloembergen damping are similar except for the explicit form of the half-width. Calculations of intensities were done with Landau-Lifshitz damping but differed from the Bloch-Bloembergen damping by only a few percent.

### Experimental Results

All efforts were made to eliminate gradients of the rf field not included in the theory. The sphere was mounted in polyfoam, inside the cavity, to prevent

stand-off effects such as those pointed out by Dillon.<sup>4</sup> No attempt was made to orient the sphere in the intensity measurements, but care was taken in polishing and grinding the sample so that the intensity did not vary substantially with orientation. The results for a MnZn ferrite sphere 1.7 mm in diameter are shown in Table V.

The first column gives the cavity mode, the second refers to Fig. 4 and indicates the position of the ferrite (black dot) with respect to the rf field, and the third column gives the orientation of the dc field with respect to the broad side of the X-band cavity, either perpendicular ( $\oplus$ ) or parallel ( $\uparrow$ ). The remaining columns give intensities, calculated and observed, for seven of the more intense lines. In the table, the comment n.o., not observed, means that the line was not seen with the sensitivity required to see the lines which were observed. The comment p.s., position sensitive, means that a very small change in position causes a very large change in intensity. The inference is that if one could position the ferrite accurately enough, one could reduce these lines below the noise level. Since elaborate and sensitive positioning equipment was not available, the sample was not positioned exactly at the point used to calculate intensity; hence there was some residual absorption.

At first glance, the agreement appears to be poor. However, when one realizes that the range of intensities is nearly  $10^7$ , the agreement seems more satisfactory. Also, the fact that no line is seen when its intensity is predicted to be zero, except those that are position sensitive, improves the agreement considerably.

One can use intensities for identification in only a

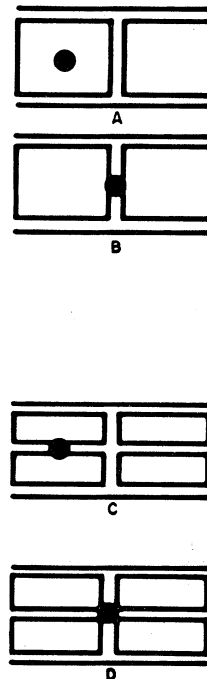


FIG. 4. Position of ferrite in cavity with respect to rf magnetic fields.

TABLE V. Observed and calculated absorption intensities,  $\Delta(1/Q)$ , for several common dc field, cavity, and ferrite configurations. Code: n.o.—not observed, p.s.—position sensitive, v.l.—very large.

| Position | Cavity mode | Position | $H_{dc}^a$ | 110             | 220          | 210             | 200             | 330            | 320             | 300           |
|----------|-------------|----------|------------|-----------------|--------------|-----------------|-----------------|----------------|-----------------|---------------|
| 1        | $TE_{106}$  | Fig. 4B  | $\uparrow$ | 0<br>0.036 p.s. | 0<br>n.o.    | 0<br>0.048 p.s. | 0<br>0.006 p.s. | 0<br>n.o.      | 0.0006<br>0.032 | 0.002<br>0.26 |
| 2        | $TE_{108}$  | Fig. 4B  | $\uparrow$ | 0<br>0.071 p.s. | 0<br>n.o.    | 0<br>0.10 p.s.  | 0<br>0.005      | 0<br>n.o.      | 0.0004<br>0.036 | 0.002<br>0.39 |
| 3        | $TE_{109}$  | Fig. 4A  | $\oplus$   | 0<br>8.7 p.s.   | 0.82<br>1.7  | 0<br>n.o.       | 9<br>428        | 0<br>n.o.      | 0<br>n.o.       | 0<br>n.o.     |
| 4        | $TE_{107}$  | Fig. 4A  | $\oplus$   | 0<br>4.0 p.s.   | 0.04<br>0.01 | 0<br>n.o.       | 7<br>232        | 0<br>n.o.      | 0<br>n.o.       | 0<br>n.o.     |
| 5        | $TE_{107}$  | Fig. 4A  | $\uparrow$ | 0<br>n.o.       | 0<br>n.o.    | 9.1<br>65       | 0<br>n.o.       | 0<br>n.o.      | 0<br>n.o.       | 0<br>n.o.     |
| 6        | $TE_{109}$  | Fig. 4A  | $\uparrow$ | 0<br>n.o.       | 0<br>n.o.    | 6.6<br>112      | 0<br>n.o.       | 0<br>n.o.      | 0<br>n.o.       | 0<br>n.o.     |
| 7        | $TE_{207}$  | Fig. 4C  | $\oplus$   | v.l.<br>v.l.    | 0<br>n.o.    | 0<br>n.o.       | 0<br>n.o.       | 0.003<br>0.005 | 0<br>n.o.       | 0<br>n.o.     |
| 8        | $TE_{106}$  | Fig. 4B  | $\oplus$   | 1700<br>2200    | 0<br>n.o.    | 0<br>n.o.       | 0<br>n.o.       | 0<br>n.o.      | 0<br>n.o.       | 0<br>n.o.     |

<sup>a</sup>  $\oplus$  indicates that the dc magnetic field is perpendicular to the broad side of the X-band cavity;  $\uparrow$  that it is parallel.

general way. Nearly all experiments are done with the ferrite at the end of a dielectric rod which distorts the rf fields. The large effect of the dielectric rod can be demonstrated by the difference in the number of lines observed when a rod is used and when polyfoam is used. With the rod in position 1, nearly 20 lines are seen; without any rod only five are seen for a YIG sample at

X band. Intensities are also useful in distinguishing between certain modes; the sample is moved slightly and intensities are observed, i.e., those marked with a  $p$  will change radically and those not so marked will remain relatively constant. Thus, although the agreement between calculations and observations of intensity is poor, intensities are helpful in identifying modes.